NUMERICAL MODEL OF VISCOUS DEBRIS FLOWS WITH DEPTH-DEPENDENT YIELD STRENGTH

Hengbin Wu [1,2], Na He [3], and Xuefu Zhang [4]

ABSTRACT

Non-Newtonian fluids such as Bingham model have been widely used to simulate the motion of viscous debris flow. The materials will flow only if shear stresses exceed its yield strength, and the integrals along the depth can be performed in the shear layer and plug layer, respectively. The pore-water pressure is considered in the rheological model according to the physical properties of viscous debris flow. In addition, the lateral pressure in horizontal direction inner debris flow is different from hydrostatic assumptions due to the presence of particles, the earth pressure coefficient with Savage-Hutter assumption is added into the governing equations. The governing equations of debris flow are solved by using Lagrange difference method, and the effects of material parameters, earth pressure coefficient and inclination angle on the runout characteristics such as velocity distribution, runout distance and deposit shape are analyzed. Numerical results show that the debris flow starts to move due to the gravity, the velocities vary almost linearly, and the rear end of debris flow moves backward because the inclination angle of plane is very small. Finally, it stops due to the basal friction force and the maximum final height locates the start position of horizontal section. Recent studies have suggested that the earth pressure coefficient mainly influences on the depth profile of granular flow, however, these phenomena have not been captured in the numerical results for debris flow perhaps due to the small inclination angle. Further studies are needed to determine the effects of earth pressure coefficient on the natural debris flow with more complex topography.

Key words: Debris flow, Bingham model, depth-integrated equations, depth-dependent yield strength, computational fluid dynamics.

1. INTRODUCTION

Debris flows are gravitational mass movements of clay, silt, sand, rock fragments mixed with air and water. The material physical characteristics of debris flow are complicated, and mainly depend on grain sizes, grain composition, clay fraction, and water contents (Takahashi 1978, 1980; Iverson 1997). The interactions between grains such as friction, slide, rotation and collision cause the rheological model of debris flow more complex. In addition, the interactions between grain and mud, and the organic materials carried by debris flow in the motion further increase the complications (Hungr *et al.* 2001; Blasio 2011).

The governing equations of debris flow are deduced by equations of open channel flow and granular flow based on computational fluid dynamics (Johnson and Rahn 1970; Jiang and LeBlond 1993; Imran *et al.* 2001a, 2001b). Johnson and Rahn (1970) have proposed that the Newtonian flow cannot reflect the non-linear relationship between the velocity and stress, and obtained the maximum speed of debris flow by using the

Bingham model. Johnson's model clearly explains several phenomena, *e.g.* the surge deposition, large grain support, and non-deformation "rigid plug" in debris flow. Takahashi (1980) has proposed the Bagnold-type dilatant fluid that attributed the formation of "surge" of debris flow to the collisions of grains. The physical model provides a critical condition of initiation and accumulation of debris flow, simultaneously explains the mechanism of phenomenon that there is no "rigid plug" in debris flow sometimes, and defines the effect of turbulent on the basal resistance model (Liu 2002).

Debris flows are accelerated downward by gravity and tend to follow steep mountain channels (Takahashi 1978; Iverson 1997; Hungr *et al.* 2001). The runout characteristics of debris flow are more complicated due to the solid/fluid duality. In a general way, the Bingham model is employed in the viscous debris flow, meanwhile, the Bagnold model is commonly employed in the dilute debris flow (Liu *et al.* 1995; Laigle and Coussot 1997; Liu 2002). For the two models mentioned above, however, it is difficult to define the critical threshold of clay content in debris flow.

Combining the results of laboratory experiments, Savage and Hutter (1989) have proposed, perhaps, the first incompressible frictional granular flow equations in the form of the depth-averaged mass and momentum balance equations along the sliding surface. A comparative analysis between Bingham model, Bagnold model, and Coulomb model with pore-water pressure is performed to analyze the motion of debris flow by Iverson (1997). Liu (2002) has proposed that the Coulomb model with pore-water pressure is different from the movement mechanism models proposed by Johnson and Rahn (1970) and Takahashi,

(1978, 1980), because it attributes the initiation mechanism of debris flow, and is mainly used to explain the failure process of debris flow in source area.

For vigorous debris flows, the spread is more predominant than the depth in scale, and translation is more significant than rotation in movement, it is reasonable to assume that the momentum equations are integrated along the vertical depth (Jiang and LeBlond 1993; Laigle and Coussot 1997; Huang and García 1997; Blasio 2011). Savage-Hutter type models have been successively extend to include the curvilinear coordinate model (Hutter *et al.* 1993; Hutter and Rajagopal 1994), mixture phases model (Iverson 1997), three dimensional model (Denlinger and Iverson 2004), erosion (entrainment) model (Luna *et al.* 2012), and two fluid model (Pitman and Lee 2005; Pudasaini *et al.* 2005; Pudasaini 2012).

In the two-phase model, debris flow and ambient fluid (air or water) are considered as a whole to simulate debris flow movement by using interface tracking technology (*e.g.* Volume of Fluid method). According to the flow characteristics of Bingham model, debris flow can flow only if shear stresses exceed its yield strength, otherwise, it moves like a rigid plug (Wu *et al.* 2013; Wu and He 2014). Based on this, we can divide the Bingham fluid into two layers: The upper is plug layer, and the lower is shear layer. There are obviously differences between the two layers, the integral equations can be carried out in the two layers, respectively.

Jiang and LeBlond (1993) have presented a numerical model that simulated the coupling of a Bingham plastic mudslide on a gentle uniform slope with the surface waves. In addition, Huang and Garcia (1997) have proposed an analytical solution for laminar mudflows and debris flows that can be modeled by a Bingham-plastic law, the method of matched asymptotic expansions was implemented to get a first-order solution. Based on the model mentioned above, Imran *et al.* (2001a, 2001b) have adopted the Lagrange finite difference method to solve the governing equations of debris flow, which is widely used to simulate debris flow movement. Two-layer model can explain many phenomena in the motion of debris flow, and show affinities with Johnson's model, because they all attribute the non-Newtonian fluids.

In this paper, the depth-dependent yield strength of debris flow is proposed according to the physical properties of viscous debris flow. The lateral earth pressure coefficient with Savage-Hutter assumption is added, the governing equations of debris flow are deduced by integrating the velocities and heights in the plug layer and shear layer, respectively. Several numerical experiments with different material parameters are implemented to analyze the effects of inclination angle, yield strength, and earth pressure coefficient on the moving time, runout distance and final deposit shape of viscous debris flow.

2. PHYSICAL PROPERTIES OF VISCOUS DEBRIS FLOW

Viscous debris flows are mixed by soil and water, generally, their densities are greater than 2000 kg/m^3,

$$\rho_d = C_v(\rho_s - \rho_w) + \rho_w \tag{1}$$

where ρ_s and ρ_w denote densities of soil and water, respectively. Their values can be obtained by laboratory experiments; C_v is volume content of soil in debris flow, its upper limit and lower limit are analyzed by practical viscous debris flow,

$$60\% \leq C_v \leq C_s \tag{2}$$

where C_s is solid particle content of debris flow,

$$C_s = 1 - n_s \tag{3}$$

where n_s is porosity of soil; for soil with well particle size distribution, C_s can reach 80%. According to Eq. (2), the value of C_v is mainly range from about 60% to 80%. The water volume fraction of debris flow $C_w = 1 - C_v$, its value is range from 20% to 40%.

For viscous debris flow, the distributions of particles size are generally wide, including soft clay, silt, fine sand, coarse sand, gravel and cobble. The porosity between soil particles are filled with mud and small amounts of air, as shown in Fig. 1. The soil particles with diameters less than 0.05 m mixed water possess a property of plasticity and shear strength τ_0; the soil particles with diameters less than the maximum suspending size D_0 are suspending because of the buoyancy of mud; for the soil particles with diameters greater than the maximum suspending size, they will be in free contact state due to the buoyancy of mud and the effective contact forces between particles. In addition, the soil particles are in contact state and have a friction angle ϕ_s.

When a viscous debris flow moves downward the inclined plane, the gravity induced shear stress is opposed by the combined effect of undrained shear strength and viscosity. The shear strength is the minimum shear stress corresponding to the first evidence of flow, *i.e.*, the value of the shear stress at zero velocity gradient. The shear strength of viscous debris flow is less than the soil's shear strength, according to the qualitative test analysis, the shear strength of viscous debris flow follows the Coulomb law,

$$\tau_y = \tau_0 + \sigma \tan \phi_m \tag{4}$$

where $\tan \phi_m$ is internal friction coefficient of viscous debris flow.
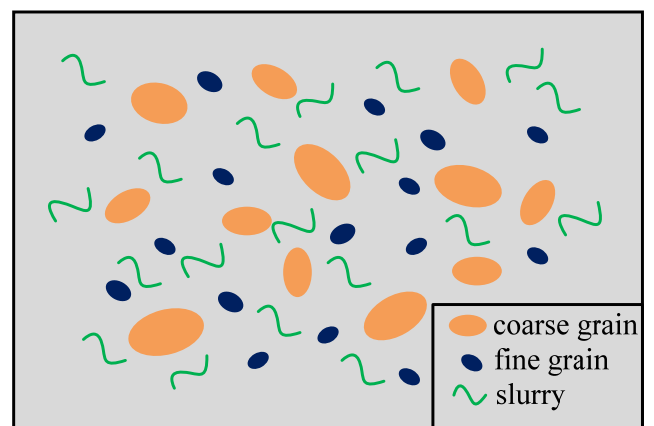

Fig. 1 Fluid structure diagram of viscous debris flow, debris flows are composed of the coarse grain, fine grain and slurry; the particles mixed water have a property of plasticity and shear strength, while the soil particles are in contact state and have a friction angle

where τ_0 is the cohesive strength. It is difficult to be measured due to the limitation of apparatus. In this paper, the cohesive strength of viscous debris flow can be replaced by shear strength of debris flow slurry τ_0; on the right side of Eq. (4), the second item is the internal friction strength of debris flow. σ is normal stress and can be replaced by the hydrostatic pressure by using the basic theory of fluid dynamics,

$$\sigma = \rho_d g h_p \tag{5}$$

where h_p is height of debris flow in the plug layer, g is gravitational acceleration, $\tan \phi_m$ can be obtained by the following method. The internal friction strength of viscous debris flow is mainly composed of the internal friction strength of soil, we can regard them as uniform,

$$\sigma \tan \phi_m = \rho_d g h_p \tan \phi_m = C_v (\rho_s - \rho_y) g h_p \tan \phi_s \tag{6}$$

where the right side of Eq. (6) is internal friction strength of soil in debris flow, $\tan \phi_s$ is the internal friction coefficient of saturated loose solid material. The viscous debris flow is composed of high content (40% to 60%) of silt and clay-size material, little sand and water, fine grainy material or soil have a smaller friction angle than the coarse sediment or debris flow. In this paper, ϕ_s is assigned as $18° \sim 20°$.

From Eq. (6), we can obtain,

$$\tan \phi_m = C_v (\rho_s - \rho_y) \tan \phi_s / \rho_c \tag{7}$$

where ρ_y is the density of solid particles in viscous debris flow: $\rho_y = P_d (\rho_s - \rho_m) + \rho_m$. P_d is the weight percentage of soil that particle sizes less than D_0, ρ_m is the density of mud excluded portions with particles sizes larger than 0.05 mm.

Iverson (1997) have proposed that pore-water pressure plays a key role in the process of debris flow movement, if the pore-water pressure p_u is considered, the yield stress is given by: $\tau_y = c + (\sigma_n - P_u) \tan \phi_m$. In order to simplify the model, we adopt the apparent friction angle proposed by Sassa (1989) to replace internal friction angle, and Eq. (4) can be rewritten as,

$$\tau_y = c + \sigma_n \tan \phi_a \tag{8}$$

where the apparent friction angle ϕ_a is obtained by $\sigma_n \tan \phi_a \approx (\sigma_n - P_u) \tan \phi_m$.

From Eq. (8), we can see that the shear stress of debris flow in the plug layer increases with the depth, the shear stress is no longer a constant, but a variable of depth dependent in the plug layer. In shear layer, the hydrostatic pressure and shear stress are also constants.

3. GOVERNING EQUATIONS OF DEBRIS FLOW

3.1 Depth Integrated Theory

Debris flow is considered as a two-dimensional, unsteady, laminar flow downward a relatively steep slope at an angle θ, and a coordinate system is defined as the *x*-axis down slope and the *y*-axis upward normal to the bed. Based on the boundary layer approximation, the governing equations of debris flow can be written as,

$$\frac{\partial u}{\partial x} + \frac{\partial v}{\partial y} = 0 \tag{9}$$

$$\frac{\partial u}{\partial t} + u \frac{\partial u}{\partial x} + v \frac{\partial v}{\partial y} = \frac{1}{\rho_d} \left(-\frac{\partial P}{\partial x} + \frac{\partial \tau}{\partial y} \right) + g \sin \theta \tag{10}$$

$$0 = -\frac{1}{\rho_d} \left(\frac{\partial P}{\partial y} \right) - g \cos \theta \tag{11}$$

where u, v are x, y directional velocities, respectively. P, τ are pressure and shear stress, respectively. ρ_d is density of debris flow.

The Herschel-Bulkley model exhibits a non-linear property and is widely used to simulate the motion of mudflow, debris flow, debris avalanche and flow slide. The rheological model can be expressed as,

$$\left| \frac{\gamma}{\gamma_r} \right|^n = \begin{cases} 0 & |\tau| < \tau_y \\ \tau / \tau_y \ \mathrm{sgn}(\gamma) & |\tau| \geq \tau_y \end{cases} \tag{12}$$

where $\gamma_r = (\tau_y / K)^{1/n}$, in which τ_y is the yield stress, K, n are empirical parameters.

As similar with other non-Newtonian fluids such as Bingham model shown in Fig. 2, the fluid will flow only if the shear stresses exceed its yield stress, otherwise, it moves like a rigid plug. Therefore, there are two layers with significantly different flow characteristics in debris flow: Plug layer and shear layer. Therefore, the integrals along the depth can be performed in the shear layer and plug layer, respectively.

Based on the boundary layer theory, the Von Karman momentum integral method and Leibniz rule are used to integrate Eq. (9) from 0 to h_s, Eq. (10) from 0 to h_s and from h_s to h, respectively. We can obtain the mass equation and momentum equations in the plug layer and shear layer,
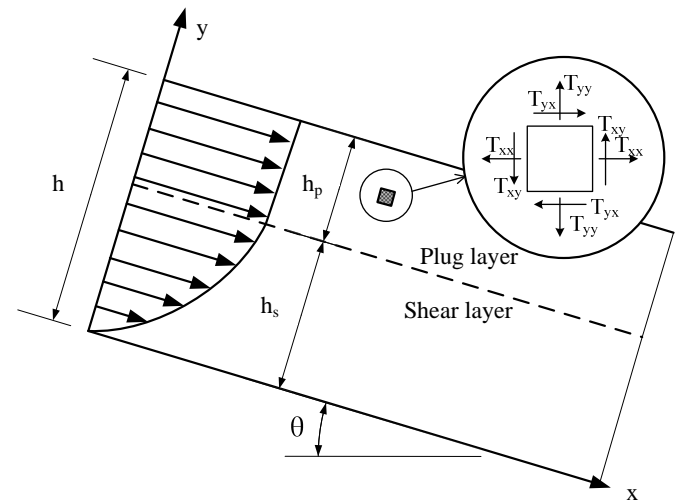

Fig. 2 Sketch of flow characteristics of non-Newtonian fluid. The fluid will flow only if the shear stresses exceed its yield stress, otherwise, it moves like a rigid plug (after Wu *et al.* 2014)

$$\frac{\partial h}{\partial t} + \frac{\partial}{\partial x}\left(u_p\left(h_p + \alpha_1 h_s\right)\right) = 0 \tag{13}$$

$$\frac{\partial}{\partial t}(u_p h_p) + u_p \frac{\partial h_s}{\partial t} + \frac{\partial}{\partial x}(u_p^2 h_p) + \alpha_1 u_p \frac{\partial}{\partial x}(u_p h_s)$$

$$= -\Delta\rho g h_p \frac{\partial h}{\partial x} + \Delta\rho g h_p S - \frac{\tau_y \, \mathrm{sgn}(h_p)}{\rho_d} \tag{14}$$

$$\alpha_1 \frac{\partial}{\partial t}(u_p h_s) - u_p \frac{\partial h_s}{\partial t} + \alpha_2 \frac{\partial}{\partial x}(u_p^2 h_s) - \alpha_1 u_p \frac{\partial}{\partial x}(u_p h_s)$$

$$= -\Delta\rho g h_s \frac{\partial h}{\partial x} + \Delta\rho g h_s S - \beta \frac{\tau_y \, \mathrm{sgn}(u_p)}{\rho_d} \left|\frac{u_p}{\gamma_r h_s}\right|^n \tag{15}$$

where h, h_s, h_p, u_p denote total height of debris flow, height in the plug layer, height and velocity of debris flow, respectively. S denotes the slope of inclined plane, $\mathrm{sgn}(u) = |u|/u$; $\Delta\rho = (\rho_d - \rho_a)/\rho_d$, where ρ_a is the density of ambient fluid.

In this paper, we assume that viscous debris flow is a steady flow with depth h, the flow velocities in the plug layer are uniform. It is further assumed that the interfacial shear stress between the debris and the ambient fluid above is negligible. The coefficients in Eqs. (13) ~ (15) are,

$$\alpha_1 = \frac{1}{u_p h_s} = \int_0^{h_s} u(y)\, dy = \frac{1 + 1/n}{2 + 1/n} \tag{16}$$

$$\alpha_2 = \frac{1}{u_p^2 h_s} = \int_0^{h_s} u^2(y)\, dy = 1 - \frac{2}{2 + 1/n} + \frac{1}{3 + 2/n} \tag{17}$$

$$\beta = (1 + 1/n)^n \tag{18}$$

$$\beta_1 = (\alpha_1 - \alpha_2)/(1 - \alpha_1) \tag{19}$$

There are four unknowns h, h_s, h_p, u_p in the governing equation of debris flow, in view of the height of debris flow is sum of the height of plug layer and shear layer: $h = h_s + h_p$. The Eqs. (13) ~ (15) can be solved with the condition mentioned above. In the process of integration along the depth, the relationship between u and u_p: $u = u_p(h_p + \alpha_1 h_s)/h$ can be acquired. In order to solve the averaged velocity and use Lagrange difference method, Eqs. (13) ~ (15) can be transformed to the following types,

$$\frac{\partial h}{\partial t} + \frac{\partial hu}{\partial x} = 0 \tag{20}$$

$$\frac{du_p}{dt} = (u - u_p)\frac{\partial u_p}{\partial x} - g\Delta\rho\cos\theta\frac{\partial h}{\partial x}$$

$$+ g\Delta\rho\sin\theta - \frac{\tau_y}{\rho_d h_p}\mathrm{sgn}(u_p) \tag{21}$$

$$\frac{du}{dt} = \frac{1}{h}\frac{\partial}{\partial x}\left(hu^2 + \beta_1 h u_p^2 - (1 + \beta_1)h u u_p\right)$$

$$+ g\Delta\rho\sin\theta - \Delta\rho g\cos\frac{\partial h}{\partial x} - \frac{\tau_y}{\rho_d h}\mathrm{sgn}(u_p) - \frac{\beta\tau_y}{\rho_d h}\left|\frac{u_p}{\gamma_r h_s}\right|^n \mathrm{sgn}(u_p) \tag{22}$$

where $\dfrac{d}{dt} = \dfrac{\partial}{\partial t} + u\dfrac{\partial}{\partial x}$.

3.2 Earth Pressure Coefficient

Let us consider debris flows traveling along a slope with laminar state, the momentum equations for the component of the velocity along slope are rewritten as,

$$\frac{1}{\rho_d}\int_0^h \frac{\partial p}{\partial x}\, dy = \frac{\rho_d g\cos\theta}{\rho_d}\int_0^h \frac{\partial(h-y)}{\partial x}\, dy \approx -gh\cos\theta\frac{\partial h}{\partial x} \tag{23}$$

If debris flow has not uniform thickness, a lateral force arises pushing from the thick to the thin parts of the debris flow, consider for simplicity the debris resting on a flat area (De Blasio 2011). At two positions x and $x + \Delta x$, the horizontal forces through a vertical slice are, respectively,

$$F(x) = \int_0^{h(x)} \rho_d g\left(h(x) - y\right) dy = \frac{\rho_d g h^2(x)}{2} \tag{24}$$

$$F(x + \Delta x) = \int_0^{h(x+\Delta x)} \rho_d g\left(h(x + \Delta x) - y\right) dy = \frac{\rho_d g h^2(x + \Delta x)}{2} \tag{25}$$

If the height of the material decreases with x, then

$$F(x + \Delta x) - F(x) \approx -\rho_d g h(x)\Delta h \tag{26}$$

We set the shear stress at the base as τ_b, Eq. (26) can be rewritten as,

$$-\rho_d g h(x)\Delta h = -\tau_b \Delta x \tag{27}$$

From Eq. (27), we obtain,

$$\tau_b = -\rho_d g h(x)\frac{\partial h}{\partial x} \tag{28}$$

It is worth noting that in the presence of a granular component, the earth pressure form can be written as,

$$-gh\cos\theta\, k_{a,p}\frac{\partial h}{\partial x} \tag{29}$$

Substituting Eq. (29) into Eq. (23), we obtain,

$$\frac{1}{\rho_d}\int_0^h \frac{\partial p}{\partial x}dy = \frac{\rho_d g\cos\theta}{\rho}\int_0^h \frac{\partial(h-y)}{\partial x}dy \approx -gh k_{a,p}\cos\theta\frac{\partial h}{\partial x} \tag{30}$$

where,

$$k_{a,p} = \begin{cases} k_a & \partial u/\partial x > \xi \\ 1.0 & |\partial u/\partial x| \le \xi \\ k_p & \partial u/\partial x < \xi \end{cases} \tag{31}$$

$$k_{a,p} = 2\left(1 \mp \sqrt{1 - (1 + \tan^2\phi_b)\cos^2\phi_a}\right)\Big/\cos^2\phi_a - 1 \tag{32}$$

where $k_{a,p}$ in Eq. (32) is the earth pressure coefficient, subscript a and p are active and passive condition, respectively. ϕ_b denotes bed friction angle, and ξ is a constant with a very small value and used as a threshold to avoid the machine precision error (Ouyang *et al.* 2013). Figure 3 shows the Mohr's circle of the stress state of debris flow. The researches on earth pressure can be divided into three models: Savage-Hutter model (Savage and Hutter 1989), Rankine model (Pirulli *et al.* 2007; Wu *et al.* 2014), and Hungr model (Hungr 1995, 2008; Hungr and McDougall 2009). In two-dimensional model, there is little distinction between the three models mentioned above, and the original Savage-Hutter model is adopted in the paper.

The velocity gradient of debris flow in the plug layer is zero, it is similar to the hydrology model (*e.g.*, shallow water equation). The earth pressure coefficient always equal 1.0 and is unnecessarily to be modified in the plug layer due to the zero velocity gradient; while, in the shear layer, the earth pressure of debris flow are transformed continuously between active, passive and static conditions, and the earth pressure coefficient is necessary to be improved due to the present of particles.

Based on the theory of computational fluid dynamics, the shear stress of viscous debris flow and earth pressure coefficient with Savage-Hutter assumption are both considered, Substituting Eqs. (8) and (30) into Eqs. (20) ~ (22), the governing equations of debris flow are given by,

Mass equation,

$$\frac{\partial h}{\partial t} + \frac{\partial hu}{\partial x} = 0 \tag{33}$$

Momentum equation in plug layer,

$$\frac{du_p}{dt} = (u - u_p)\frac{\partial u_p}{\partial x} - g\Delta\rho\cos\theta\frac{\partial h}{\partial x} + g\Delta\rho\sin\theta$$
$$- \frac{c + \Delta\rho g h_p \cos\theta\tan\varphi_a}{\rho_d h_p}\operatorname{sgn}(u_p) \tag{34}$$

Momentum equation in shear layer,

$$\frac{du}{dt} = \frac{1}{h}\frac{\partial}{\partial x}\left(hu^2 + \beta_1 h u_p^2 - (1+\beta_1)huu_p\right)$$
$$+ g\Delta\rho\sin\theta - k_{a,p}\Delta\rho g\cos\theta\frac{\partial h}{\partial x}$$
$$- \frac{(c + \Delta\rho g h_p \cos\theta\tan\phi_a)}{\rho_d h}\left(1 + \left|\frac{u_p}{\gamma_r h_s}\right|^n\right)\operatorname{sgn}(u_p) \tag{35}$$

From Eqs. (33) ~ (35), we see that for the momentum equation, the acceleration of debris flow depends on the following factors, (1) the spatial variation of *x* momentum fluxes; (2) driving gravitational force; (3) dissipative internal friction force; and (4) dissipative basal friction force, its direction depends on the velocity of debris flow.
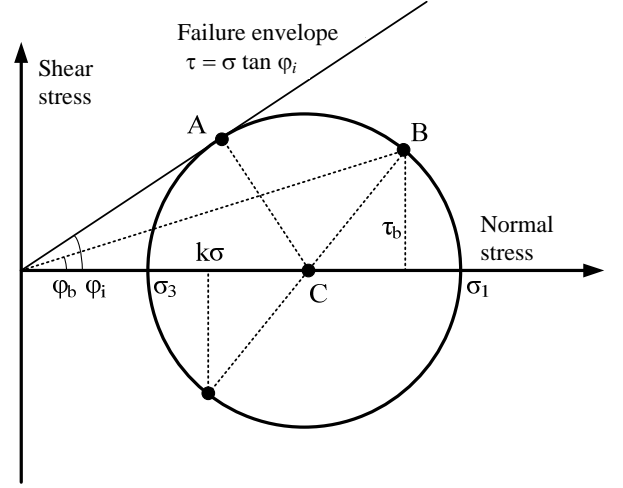

Fig. 3   **Mohr's circle representing the stress state in an element of material undergoing general shearing in the passive regime and basal shearing at the contact between the material and the base of the flow (after Savage and Hutter 1989; Hungr 2008)**

4. NUMERICAL SCHEME

For depth averaged equations, the numerical method can be divided into three types: Adding a viscous coefficient, using a high resolution algorithm, and developing the finite volume method. Equations (33) ~ (35) also can be solved by using the algorithm of depth averaged equations. According to the Lagrange difference method (Savage and Hutter 1989; Imran *et al.* 2001a; Imran *et al.* 2001b; Hutter and Rajagopal 1994), as shown in Fig. 4, the debris flow is divided into a number of cells, and the index *i* and *j* are denoted as the cell centers and cell boundary points, respectively.

In the initial state, we give u and u_p a very small value, the velocities in the boundary of mesh are denoted by u_j and u_{pj}, respectively; the velocities of node can be obtained by $u_i = 1/2(u_j + u_{j+1})$ and $u_{pi} = 1/2(u_{pj} + u_{p(j+1)})$.

The density of debris flow is constant, the mass conservation equation can be transferred to the condition that the area of element is constant, in other words, because the right part of Eq. (20) equal zero, integrating it from x_j to x_{j+1} can be a constant, and Eq. (20) can be rewritten as,

$$\int_{x_j}^{x_{j+1}}\left(\frac{\partial h}{\partial t} + \frac{\partial hu}{\partial x}\right)dx = \frac{d}{dt}\int_{x_j}^{x_{j+1}}h\,dx$$
$$= 0 \Rightarrow h_i(x_{j+1} - x_j) = \text{const} \tag{36}$$

According to the mass conservation equation, we can obtain the center height of element:

$$h_i^{t+\Delta t} = h_i^t \frac{x_{j+1}^t - x_j^t}{x_{j+1}^{t+\Delta t} - x_j^{t+\Delta t}} \tag{37}$$

After Δt, the displacement of grid boundary x_{j+1}^t,

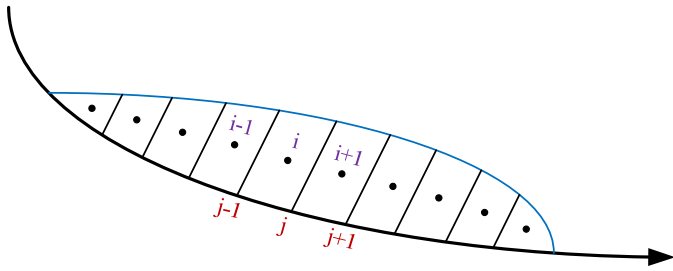$$x_{j+1}^t = x_j^t + u_j^{(n-1/2)}\Delta t \tag{38}$$

Fig. 4   Sketch of numerical method, the indexes i and j are cell centers and cell boundary points, respectively

The difference scheme of momentum equations in the plug layer and shear layer are listed as following Eqs. (39) and (40), respectively,

$$u_{pj}^{t+\Delta t} = u_{pj}^{t} + \Delta t \left((u - u_p)\frac{\partial u_p}{\partial x} - g\Delta\rho\cos\theta\frac{\partial h}{\partial x} \right.$$
$$\left. + g\Delta\rho\sin\theta - \frac{c + \Delta\rho g h_p \cos\theta\tan\varphi_a}{\rho_d h_p}\text{sgn}(u_p) \right) \tag{39}$$

$$u_j^{t+\Delta t} = u_j^{t} + \Delta t \left(\frac{1}{h}\frac{\partial}{\partial x}\left(hu^2 + \beta_1 h u_p^2 - (1+\beta_1)huu_p \right) \right)$$
$$+ g\Delta\rho\sin\theta - k_{a,p}\Delta\rho g \cos\frac{\partial h}{\partial x}$$
$$- \frac{(c + \Delta\rho g h_p \cos\theta\tan\varphi_a)}{\rho_d h}\left(1 + \left|\frac{u_p}{\gamma_r h_s}\right|^n \right)\text{sgn}(u_p) \tag{40}$$

Notice that the sign of earth pressure coefficient are defined by,

$$k_{a,p}^{t+\Delta t} = \begin{cases} k_a & (u_{j+1}^t - u_j^t) > \xi \\ 1.0 & |u_{j+1}^t - u_j^t| \leq \xi \\ k_p & (u_{j+1}^t - u_j^t) < \xi \end{cases} \tag{41}$$

In order to hold the stability of arithmetic, a viscosity item is added into the velocities of node,

$$\begin{cases} u_j = u_j + v_m(u_{j+1} - 2u_j + u_{j-1}) \\ u_{pj} = u_{pj} + v_m(u_{p(j+1)} - 2u_{pj} + u_{p(j-1)}) \end{cases} \tag{42}$$

where $v_m = v_c\dfrac{h_{j+1} - 2h_j + h_{j-1}}{h_{j+1} + 2h_j + h_{j-1}}$. v_c is artificial viscosity coefficient, and can be selected to be a small value.

It is worth noting that there are four unknowns h, h_s, h_p, u_p in the governing equations of debris flow, the relationship between u and u_p: $u = u_p (h_p + \alpha_1 h_s)/h$, can be converted to the following form,

$$u_j = \begin{cases} u_{pj} & u_j / u_{pj} > 1 \\ \alpha_1 u_{pj} & u_j / u_{pj} \leq \alpha_1 \end{cases} \tag{43}$$

$$h_p = h \cdot \left(\frac{u}{u_p} - \alpha_1 \right)\Big/(1-\alpha_1) \tag{44}$$

We give the initial velocity in the plug layer u_p a very small value, the total velocity u can be obtained by Eq. (43); the depth in the plug layer h_p can also be determined according to the relationship between u and u_p; meanwhile, the depth in the shear layer h_s can be obtained by $h_s = h - h_p$.

The time step is set as $0.001\sqrt{\Delta x / 9.81}$, Δx denotes grid size. The artificial viscosity coefficient in the numerical approach is set as 0.03. The calculation will stop if the maximum velocity of debris flow is less than 0.01m/s. The details of Lagrange difference method can refer to Savage and Hutter (1989), Imran *et al.* (2001a), Imran *et al.* (2001b) and Hutter and Rajagopal (1994).

5.   NUMERICAL MODEL AND RESULTS

5.1   Release of Debris Flow on an Inclined Plane with Flat Gradient

Release of debris flow moving on an inclined plane is performed in this paper. h_0 and L_0 denote the maximum initial height and length of debris flow, respectively, the initial pile of debris flow to be released is assumed to have a thickness $h(x)$ that varies in the shape of a parabola with length and maximum height: $h(x) = h_0 - 4h_0((x - L/2)/L)^2$. Figure 5 shows the numerical model of debris flow, the maximum initial height and length of debris flow are 20 m and 100 m, respectively; The angle and length of inclined plane are 15° and 1,000 m, respectively; the horizontal length and fillet radius are 2,000 m and 1,000 m, respectively. In order to ensure the computational accuracy, the grid size is set as 5.0 m. The density of debris flow and air are 1,800 kg/m³ and 1.0 kg/m³, respectively. The details of physical quantities in the numerical models are listed in Table 1.

The numerical results have been scaled by L_0 for length, H_0 for height (depth) and $U_0 = \sqrt{gA^{0.5}}$ for velocity, respectively. A denotes the total cell's area of debris flow and remains constant due to the invariant density. The initial length and height are $L_0 = 100$ m, $H_0 = 20$ m, respectively. We can obtain the volume per unit width $A = 4000/3$ m², and the velocity scale $U_0 = 19.11$ m/s. Note that U_0 is a velocity scale and not the actual velocity of any debris flow. Table 2 lists the predicted results of the original and depth-dependent yield strength models, Case 1 represents the original model, *i.e.*, the yield strength remains constant, while, Case 2 represents the modified model, and has a depth-dependent yield strengths.

Figure 6 shows the computed results of the depth-dependent yield strengths at several typical times. The solid and short dash lines represent the depth profile and velocity distribution, respectively, at the last panel, dash-dot line denote the front velocity of debris flow. From Fig.6, we see that debris flow moving fast at the beginning due to the gravity; the velocity of debris flow will reduce and gradually tend to be zero with the influences of basal friction force. At the early stage, the velocities of debris flow vary linearly, similar arguments for granular flow with Coulomb

friction law have reported by Tai *et al.* (2002). Finally, the debris flow stops because potential energy transfers to kinetic energy and converts to internal energy by overcoming the basal friction force. The maximum final height locates the start position of horizontal plane. From the front velocity of debris flow at the last panel, it can be seen that the front velocity of debris flow accelerates quickly, then remains approximately constant until it reaches the curved transition, and finally stops moving from the front to tail in the runout zone.

Table 1   Physical quantities in the numerical models

Physical quantities	Value	Physical quantities	Value
Density of debris flow	1,800 kg/m^3	Inclination angle	15°
Density of ambient air	1.0 kg/m^3	Length of inclined plane	1,000 m
Initial height of debris flow H_0	20 m	Length of horizontal plane	2,000 m
Initial length of debris flow L_0	100 m	Fillet radius	1,000 m
Initial velocity of debris flow	0 m/s	Bed friction angle	10°
Empirical parameter n	1.0	Artificial viscosity coefficient v_c	0.03
Reference strain rate γ_r	2.5	Threshold value ξ	10e−5

Table 2   Predicted results of the original and depth-dependent yield strength models

Run no.	Inclination angle	Earth pressure coefficient[a]	Shear strength[b]		Runout time[c]	Runout distance
			Cohesion	Internal friction angle		
Case 1	15°	1.0	600 Pa		110.60 s	13.31 L_0
Case 2	15°	S-H assumption	500 Pa	15°	113.97 s	13.42 L_0

[a] Case 1 employs the hydrostatic assumption, and Case 2 employs the Savage-Hutter assumption with a bed friction angle of 10°;

[b] Case 1 has a constant shear strength, and Case 2 has a depth-dependent yield strengths;

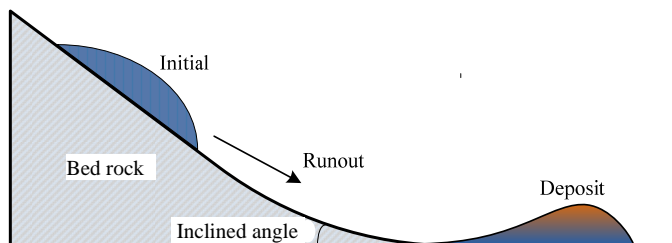[c] Time at which the maximum velocity reaches negligible value.

Fig. 5   Numerical model of debris flow, debris flow will move from initial condition due to gravity; then stop because of the potential energy transfers to kinetic energy and is converted to internal energy by overcoming the basal friction
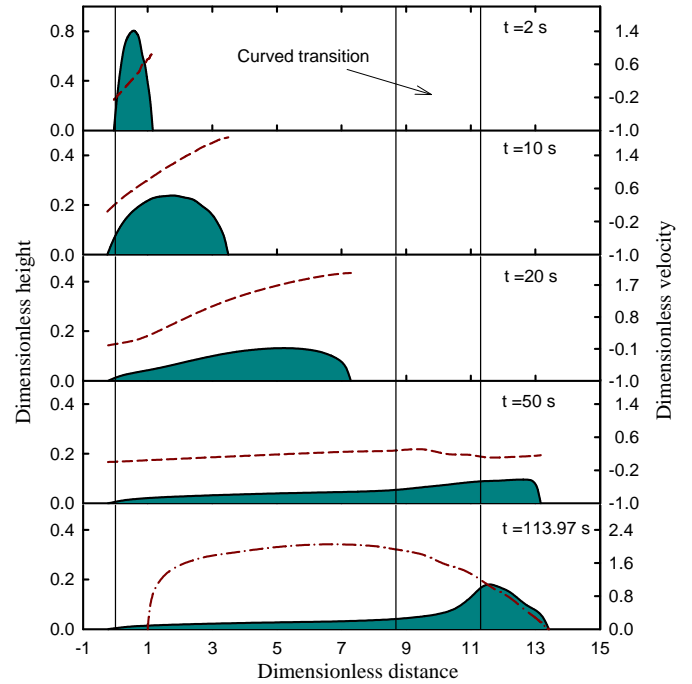

Fig. 6   The computed results of Case 2 at 2s, 10s, 30s, 50s and 113.97s, respectively

Figure 7 shows the velocity distributions of debris flow at several typical times, it can be seen that the tail of debris flow moves backward due to the gravity, meanwhile, the front of debris flow moves forward quickly. The velocities of debris flow in the inclined plane vary almost linearly. When the debris flow reaches the curved transition, the velocity decreases in the approaching front. Finally, the debris flow reaches the horizontal section. The maximum moving time and runout distance are about 113.97 s and 13.42 *L*, respectively. The maximum dimensionless velocity at the several typical times are about 2.0, because the numerical model is not the natural debris flow, the maximum velocity of debris flow perhaps is much larger than it really is.

Figure 8 shows the final deposit shapes of the original and modified models. We see that the law of motion and maximum deposit height of the modified model are close to that of the original model. The predicted runout distance of the modified model is slightly greater than that of the original model. The material parameters adopted in the paper is not the accurate parameters of real debris flow, our goal is to analyze the movement law of debris flow with different models and not to exactly predict the natural debris flow. The similar results have validated the reasonableness and reliability of predicted results with depth dependent yield strength model.

5.2   Role of Earth Pressure Coefficients

In order to analyze the effect of earth pressure coefficient on the motion of debris flow, several bed friction angles are adopted to simulate the moving time and runout distance. Hydrostatic assumptions are employed in Case 1, *i.e.*, the earth pressure coefficient equal 1.0; while the bed friction angles equal 8°, 10° and 14.5° in Case 2, 3, and 4, respectively. The runout characteristics are listed in Table 3, we see that the active and passive values of

earth pressure coefficient approach 1.0 with increment of bed friction angle, the runout distance increases with increasing bed friction angle. The moving times of several cases have no significant regularity due to the terminal criterion adopted in the numerical approach. It is perhaps because the deposit will continue to creep very slowly even after rapid flow has ceased.

Table 3   Runout characteristics of debris flow[a]

Run no.	Inclination angle	Internal friction angle	Bed friction angle	k_a	k_p	Runout time	Runout distance
Case 1[b]	15°	15°	–	1.0	1.0	127.79 s	13.46 L_0
Case 2	15°	15°	8°	0.67	1.62	116.75 s	13.42 L_0
Case 3	15°	15°	10°	0.73	1.56	113.97 s	13.42 L_0
Case 4	15°	15°	14.5°	0.99	1.29	123.97 s	13.43 L_0

[a] k_a and k_p denote the active and passive values of earth pressure coefficient, respectively;

[b] Hydrostatic assumptions are employed in Case 1, *i.e.*, the earth pressure coefficient in Case 1 equals 1.0.
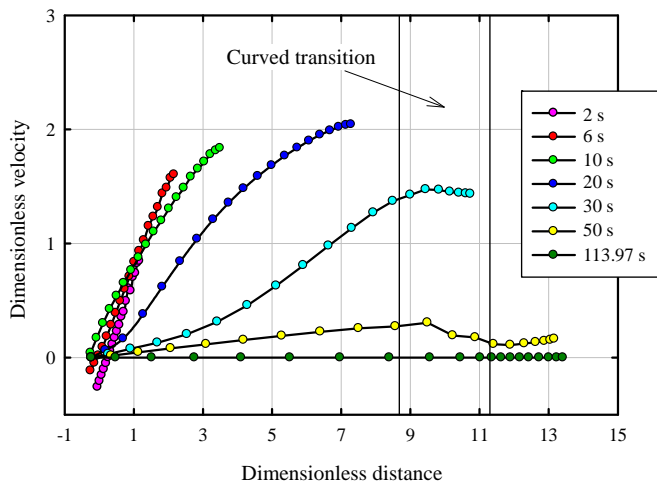

Fig. 7   Velocity distributions of debris flow at typical times
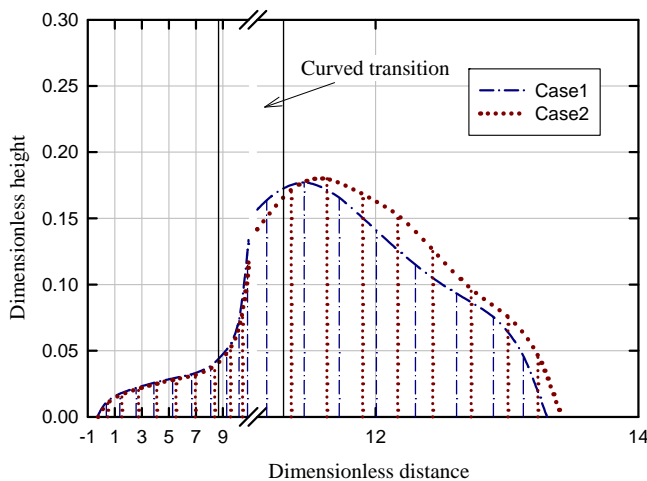

Fig. 8   Final deposit shapes of the two cases

Using the conclusions drawn by Tai *et al.* (2002), Pirulli *et al.* (2007) and Savage and Hutter (1991), the earth pressure coefficient mainly influences on the depth profile of granular flow, and has no significantly influences on the moving time and runout distance. The front part of final deposits of debris flow with different earth pressure coefficients are shown in Fig. 9, we see that the final deposits are very similar; the more bed friction angle approaches the internal friction angle, the more deposition profile gets close to the case with hydrostatic assumption. Because the inclination angle of debris flow is relatively small, the influences of the earth pressure coefficient on the runout characteristics for debris flow are not obvious than large natural rock avalanches and landslides.

5.3   Role of Empirical Parameter *n*

If the empirical parameter *n* equals 1.0, the Herschel-Bulkley model will reduce to the Bingham model, to analyze the effect of *n* on the movement of debris flow, four values of *n* ranging from 0.7 to 1.0 are chosen in the numerical experiments (see Table 4). It is known that the smaller the *n* value, the larger the runout distance of debris flow, however, the runout times have no significant regularity as mentioned above. We can conclude that the computing time cannot exactly describe the real runout time if the depth averaged equations are solved by Lagrange difference methods, especially for the complex topography. By contrast, the runout distance and depth profile are more reliable.

Table 4   Role of empirical parameter *n* in the numerical simulations

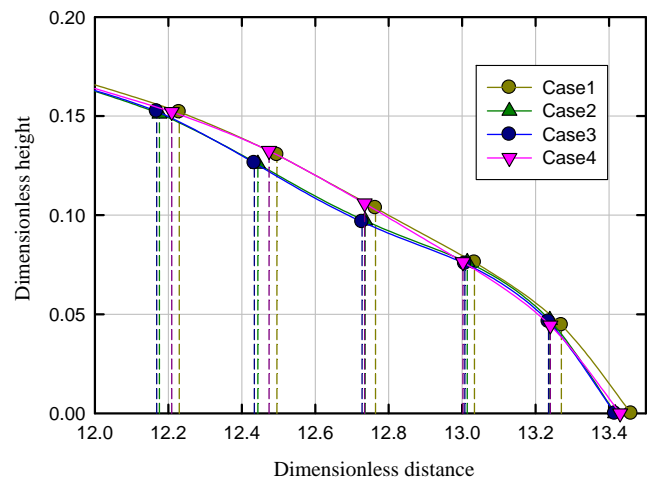| Run no.	Inclination angle	Empirical parameter *n*	Shear strength		Runout time	Runout distance
			Cohesion	Internal friction angle		
Case 1	15°	1	500 Pa	15°	113.97 s	13.42 L_0
Case 2	15°	0.9	500 Pa	15°	159.20 s	14.26 L_0
Case 3	15°	0.8	500 Pa	15°	110.26 s	15.35 L_0
Case 4	15°	0.7	500 Pa	15°	101.39 s	16.79 L_0

Fig. 9   Final deposit profiles of the four cases

5.4 Role of Inclination Angle of Plane

The inclination angle of plane plays an important role for the runout characteristics, we conduct a numerical case with a inclination angle of 10° to analyze the effect of inclination angle on the runout distance, the fillet radius is set as 1000 m, and the corresponding curved transition is shorter than that of the original case. The computed results are listed in Table 5, we see that the runout distance decreases with increasing inclination angle, and the final deposition shapes are very similar. Combined the Figs. 6 and 10, the maximum final heights of debris flow nearly locate in the start position of horizontal plane, the rear end of debris flow slightly moves backward. This phenomena depends on the nature of non-Newtonian fluid and are different with Coulomb and corresponding advanced rheological models (Pudasaini *et al.* 2005; Pudasaini 2012). Figure 11 shows the velocity distribution of Case 2, it is known that the maximum velocity of Case 2 is significantly less than that of Case 1, and this feature influences the runout distance of debris flow.

Table 5   Runout characteristics of debris flow

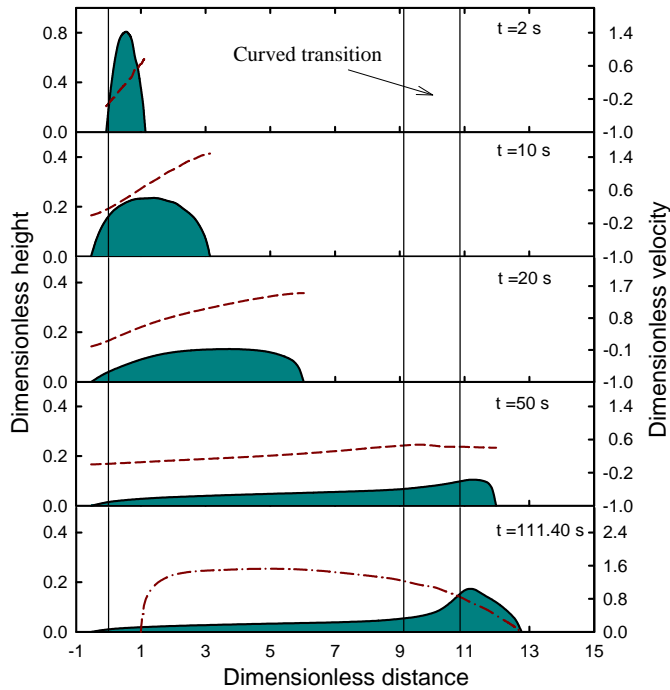| Run no.	Inclination angle	Bed friction angle	Shear strength		Runout time	Runout distance
			Cohesion	Internal friction angle		
Case 1	15°	10°	500 Pa	15°	113.97 s	13.42 L_0
Case 2	10°	10°	500 Pa	15°	111.40 s	12.76 L_0

Fig. 10   The computed results of Case 2 at 2 s, 10 s, 30 s, 50 s and 111.40 s, respectively
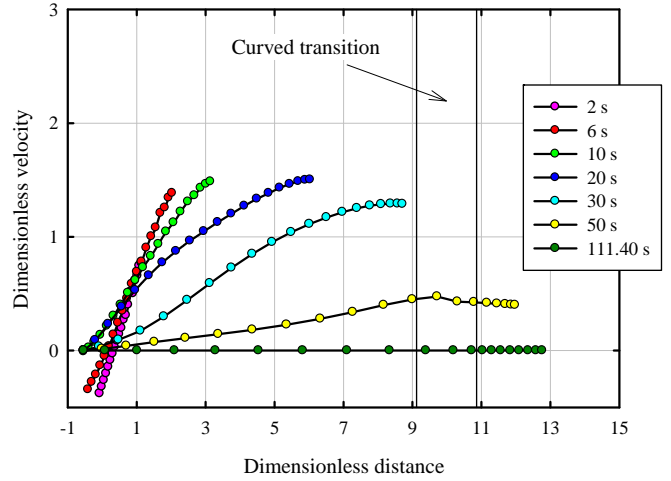

Fig. 11   Velocity distributions of debris flow at typical times

6. CONCLUSIONS

Based on physical characteristics of viscous debris flow, the basal friction item is improved by introducing the shear stress index. In addition, the earth pressure coefficient with Savage-Hutter assumption is taken into considered in the shear layer, and the governing equations of debris flow are established. The model is solved by Lagrange difference method and verified by several numerical models. Our goal is not to analyze the real debris flow, but to implement the contrastive analysis of the modified and original models, and further study the sensitivity of material parameters. Numerical results show that the debris flow starts to move due to the gravity, and the velocities vary almost linearly, this is in line with those already described in Pudasaini *et al.* (2005), and Pudasaini and Hutter (2007). The rear end of debris flow moves backward because the inclination angle of plane is very small. The runout characteristics of the modified model with a depth dependent yield strength are very close to that of the original model.

The earth pressure coefficient has a significant influence on the movement of granular flow, especially on the large rock avalanches and natural landslides. Several cases with different bed friction angles are performed, and the numerical results show the effect of bed friction angle on the runout distance is insignificant. As described in Pirulli *et al.* (2007) and Hungr (2008), the earth pressure coefficient mainly influences on the depth profile, however, these phenomena have not been captured in the numerical results for debris flow perhaps due to the small inclination angle. It can be further studied for the relatively steep or complex topography. In addition, the computing time is not the exactly moving time of debris flow and only used as a reference, if the terminal criterion is set as the maximum velocity less than a very small value. It is perhaps because the deposit will continue to creep very slowly even after rapid flow has ceased.

The empirical parameter n has significantly influences on the runout distance, the rheological parameters are determined to be worth of attention by fitting the laboratory tests and observations. Further, the effects of inclination angle of plane on the runout characteristics are obvious. The numerical models adopted in the paper are simple and needed to further be applied into the practical engineering with depth dependent yield strength model.

ACKNOWLEDGEMENTS

REFERENCES

De Blasio, F.V. (2011). *Introduction to the Physics of Landslides: Lecture Notes on the Dynamics of Mass Wasting*, Springer, Berlin.

Denlinger, R.P. and Iverson, R.M. (2004). "Granular avalanches across irregular three-dimensional terrain: 1. Theory and computation." *Journal of Geophysical Research: Earth Surface* (2003-2012), **109**(F1).

Huang, X. and García, M.H. (1997). "A perturbation solution for Bingham-plastic mudflows." *Journal of Hydraulic Engineering*, **123**(11), 986−994.

Hutter, K., Siegel, M., Savage, S.B., and Nohguchi, Y. (1993). "Two-dimensional spreading of a granular avalanche down an inclined plane Part I. theory." *Acta Mechanica*, **100**(1-2), 37−68.

Hutter, K. and Rajagopal, K.R. (1994). "On flows of granular materials." *Continuum Mechanics and Thermodynamics*, **6**(2), 81−139.

Hungr, O. (1995). "A model for the runout analysis of rapid flow slides, debris flows, and avalanches." *Canadian Geotechnical Journal*, **32**(4), 610−623.

Hungr, O., Evans, S.G., Bovis, M.J., and Hutchinson, J.N. (2001). "A review of the classification of landslides of the flow type." *Environmental & Engineering Geoscience*, **7**(3), 221−238.

Hungr, O. (2008). "Simplified models of spreading flow of dry granular material." *Canadian Geotechnical Journal*, **45**(8), 1156−1168.

Hungr, O. and McDougall, S. (2009). "Two numerical models for landslide dynamic analysis." *Computers & Geosciences*, **35**(5), 978−992.

Imran, J., Harff, P., and Parker, G. (2001a). "A numerical model of submarine debris flow with graphical user interface." *Computers & Geosciences*, **27**(6), 717−729.

Imran, J., Parker, G., Locat, J., and Lee, H. (2001b). "1D numerical model of muddy subaqueous and subaerial debris flows." *Journal of Hydraulic Engineering*, **127**(11), 959−968.

Iverson, R.M. (1997). "The physics of debris flows." *Reviews of Geophysics*, **35**(3), 245−296.

Jiang, L. and LeBlond, P.H. (1993). "Numerical modeling of an underwater Bingham plastic mudslide and the waves which it generates." *Journal of Geophysical Research: Oceans* (1978–2012), **98**(C6), 10303−10317.

Johnson, A.M. and Rahn, P.H. (1970). "Mobilization of debris flows." *Zeitschrift fur Geomorphologie*, **9**(Suppl), 168−186.

Laigle, D. and Coussot, P. (1997). "Numerical modeling of mudflows." *Journal of Hydrologic Engineering*, **123**(7), 617−623.

Liu, G., Cui, Z., and Wang, X. (1995). Sedimentary macrostructures of debris flows and their formation mechanism, *Geological Review*, **41**(2): 159−164 (in Chinese).

Liu, X. (2002). "An overview of foreign debris flow mechanism models." *Journal of Catastrophology* (in Chinese), **17**(4), 1−6.

Luna, B.Q., Remaître, A., van Asch, T.W., Malet, J.P., and van Westen, C.J. (2012). "Analysis of debris flow behavior with a one dimensional run-out model incorporating entrainment." *Engineering Geology*, **128**, 63−75.

Ouyang, C., He, S., Xu, Q., Luo, Y., and Zhang, W. (2013). "A MacCormack-TVD finite difference method to simulate the mass flow in mountainous terrain with variable computational domain." *Computers & Geosciences*, **52**, 1−10.

Pirulli, M., Bristeau, M.O., Mangeney, A., and Scavia, C. (2007). "The effect of the earth pressure coefficients on the runout of granular material." *Environmental Modelling & Software*, **22**(10), 1437−1454.

Pitman, E.B., and Lee, L. (2005). "A two-fluid model for avalanche and debris flows." *Philosophical Transactions of the Royal Society A: Mathematical, Physical and Engineering Sciences*, **363**(1832), 1573−1601.

Pudasaini, S.P., Wang, Y., and Hutter, K. (2005). "Modelling debris flows down general channels." *Natural Hazards and Earth System Science*, **5**(6), 799−819.

Pudasaini, S.P. and Hutter, K. (2007), *Avalanche Dynamics: Dynamics of Rapid Flows of Dense Granular Avalanches*. Springer, New York, USA.

Pudasaini, S.P. (2012). "A general two-phase debris flow model." *Journal of Geophysical Research: Earth Surface* (2003-2012), **117**(F3).

Sassa, K. (1989). "Geotechnical classification of landslides." *Landslide News*, **3**, 21−24.

Savage, S.B. and Hutter, K. (1989). "The motion of a finite mass of granular material down a rough incline." *Journal of Fluid Mechanics*, **199**, 177−215.

Savage, S.B. and Hutter, K. (1991). "The dynamics of avalanches of granular materials from initiation to runout. Part I: Analysis." *Acta Mechanica*, **86**(1-4), 201−223.

Tai, Y.C., Noelle, S., Gray, J.M. N. T., and Hutter, K. (2002). "Shock-capturing and front-tracking methods for granular avalanches." *Journal of Computational Physics*, **175**(1), 269−301.

Takahashi, T. (1978). "Mechanical characteristics of debris flow." *Journal of the Hydraulics Division*, **104**(8), 1153−1169.

Takahashi, T. (1980). "Debris flow on prismatic open channel." *Journal of the Hydraulics Division*, **106**(3), 381−396.

Wu, H.B., He, S.M., Zhang, W.C., and Wang, D.P. (2013). "Runout and impact analysis of flow slide based on computational fluid dynamics." *Electronic Journal of Geotechnical Engineering*, **18**(Q), 3695−3717.

Wu, H.B., He, Z.P., Mao, H.T., and Zhou, T.Q. (2014). "On the motion of debris flow based on the energy conservation law." *Electronic Journal of Geotechnical Engineering*, **19**(S), 4555−4573.

Wu, H.B. and He, S.M. (2014). "An improved mathematical model for geological analysis of debris flow." *Journal of Geography and Geology*, **6**(1), 129−138.